From Coating to Dopant: How the Transition Metal Composition Affects Alumina Coatings on Ni-rich Cathodes

Binghong Han[1*], Baris Key[1], Saul H. Lapidus[2], Juan C. Garcia[3], Hakim Iddir[3], John T. Vaughey[1], Fulya Dogan[1]

1. Chemical Sciences and Engineering Division, 2. X-ray Sciences Division, 3. Materials Science Division, Argonne National Laboratory, Argonne, Illinois 60439, United States

*: binghong.han@anl.gov

ABSTRACT

Surface alumina coatings have been shown to be an effective way to improve the stability and cyclability of cathode materials. However, a detailed understanding of the relationship between the surface coatings and the bulk layered oxides is needed to better define the critical cathode–electrolyte interface. In this paper, we systematically studied the effect of the composition of Ni-rich $LiNi_xMn_yCo_{1-x-y}O_2$ (NMC) on the surface alumina coatings. Changing cathode composition from $LiNi_{0.5}Mn_{0.3}Co_{0.2}O_2$ (NMC532) to $LiNi_{0.6}Mn_{0.2}Co_{0.2}O_2$ (NMC622) and $LiNi_{0.8}Mn_{0.1}Co_{0.1}O_2$ (NMC811) was found to facilitate the diffusion of surface alumina into the bulk after high-temperature annealing. Using a variety of spectroscopic techniques, Al was seen to have a high bulk compatibility with higher Ni/Co content and low bulk compatibility was associated with Mn in the transition metal layer. It was also noted that the cathode composition affected the observed morphology and surface chemistry of the coated material, which has an effect on electrochemical cycling. The presence of a high surface Li concentration and strong alumina diffusion into the bulk lead to a smoother surface coating on NMC811 with no excess alumina aggregated on the surface. Structural characterization of pristine NMC particles also suggests surface Co segregation, which may act to mediate the diffusion of the Al from the surface to the bulk. The diffusion of Al into the bulk was found to be detrimental to the protection function of surface coatings leading to poor overall cyclability, indicating the importance of compatibility between surface coatings and bulk oxides on the electrochemical performance of coated cathode materials. These results are important in developing a better coating method for synthesis of next generation cathodes materials for lithium ion batteries.

KEYWORDS

Cathode Materials; NMC; Compositional Effect; Aluminum Insertion; Alumina Coating; Aluminum Doping; MAS NMR; TEM.

I. INTRODUCTION

The development of new lithium-ion batteries with longer cycle life and higher energy density is critical for decreasing the weight, costs, and environmental impact of portable electronic devices and electric or hybrid vehicles[1-3]. Recently, the new cathode material family, $LiNi_xMn_yCo_{1-x-y}O_2$ (NMC), has created great commercial interest and has been utilized by numerous zero-emission or hybrid electric vehicles[3]. Unlike the traditional cathode materials such as $LiCoO_2$ (LCO) or $LiMn_2O_4$ (LMO), NMC cathode materials have a more complex cation arrangement that allows changes in the transition metal composition to be optimized for better energy density, power density, cycle life and thermal stability[4-12]. Among NMC materials, the Ni-rich cathodes have been intensively studied, such as $LiNi_{0.5}Mn_{0.3}Co_{0.2}O_2$ (NMC532), $LiNi_{0.6}Mn_{0.2}Co_{0.2}O_2$ (NMC622) and $LiNi_{0.8}Mn_{0.1}Co_{0.1}O_2$ (NMC811), because the high Ni content brings higher specific capacities and relatively lower costs than more Co-rich NMC materials [4-5, 13]. On the other hand, the relatively low content of manganese and cobalt in Ni-rich NMC materials has been associated with lower thermal stability and electrochemical cyclability due to the intrinsic structural instability of formally tetravalent nickel[14-16]. While tuning the transition metal ratios in NMC materials is an important approach to developing a balanced performance between the capacity and stability varying just the composition is not enough to optimize the performance of NMC cathodes [5-8, 15-17]. Particularly when operated at higher voltages (> 4.6 V), NMC cathodes often suffer from electrolyte decomposition and the degradation of oxide structure due to the reductive nature of cathode-electrolyte reactions, transition metal dissolution, oxygen leaching, and transition metal rearrangement[4, 18]. To solve the stability issue, several surface coatings, such as SiO_2[19], TiO_2[20], Li_2ZrO_3[21], and in particular Al_2O_3[22-27], have been studied and were shown to strongly influence the cyclability of NMC by mechanisms that have included suppressing surface reactivity and the chemical and structural transitions during the electrochemical cycling.

Despite the observation that an Al_2O_3 coating is a practical way to increase the cyclability of NMC, a comprehensive understanding of the interaction between the NMC surface and Al_2O_3 coating is still missing. This is because the low coating content of a thin layer and a complicated coating-core interface often make it hard to investigate the exact surface coating composition and its influence on the bulk cathode structure after a series of coating and thermal treatments. The lack of a detailed understanding of the surface structure of Al_2O_3-coated NMC materials has hampered the further study of the surface-electrolyte interaction, solid electrolyte interface (SEI) formation, and the capacity degradation on electrochemical cycling as this materials combination is regarded as a baseline for coated cathode materials. In our previous studies, we used a combination of electron microscopy and solid state Nuclear Magnetic Resonance (NMR) techniques to investigate the local chemical environments, coating morphologies and surface atomic structures of both Al-doped ($LiNi_{1-y-z}CoyAl_zO_2$ (NCA) and NMC)[28] and

Al-coated (LCO and NMC)[29] cathode materials. In these studies, we noted the incompatibility between Al and Mn cations in the bulk of NMC and the higher solubility and bulk compatibility of Al_2O_3 in Co-rich materials in both studies. In general, the presence of Mn cations in NMC hinders Al(III)/Al_2O_3 to directly substitute into the lattice or diffuse from the surface coating into the core after high-temperature treatment[28-29]. In comparison, Al(III)/Al_2O_3 can be easily substituted into NCA and LCO, which do not contain any Mn cations [28-29]. Although commonly used, the effect of composition on the aluminum coating and doping in Ni-rich NMC cathodes is yet to be clearly understood and a more detailed compositional study on NMC materials is warranted to provide insights that can lead to further improvements in cathode capacity and cyclability.

In this work, we systematically investigated the influence of bulk NMC compositions on the Al_2O_3-coated cathode materials. A series of Al_2O_3-coated NMC532, NMC622 and NMC811 were prepared using a wet coating method and treated under various sintering conditions. Scanning Electron Microscopy (SEM), Transmission Electron Microscopy (TEM), high-resolution X-ray diffraction (HRXRD) and solid state NMR characterization techniques are used in combination to reveal the surface elemental distributions, local chemical and atomic structure, surface species, and lattice Al diffusion before and after the coating process. High-temperature annealing was found to lead to a thinner and more closely attached surface coatings with the formation of $LiAlO_2$ phase on all NMC particles. In contrast to NMC532, the low Mn content in NMC622 and NMC811 was found to facilitate the transfer of alumina from the surface into the bulk after high-temperature annealing, and the nature of Al local environment suggests the Co segregation on the surface, which plays a crucial role in the aluminum diffusion process. The blocking effect of Mn cations on Al cation insertion is further confirmed by the density functional theory (DFT) calculations. These discoveries demonstrate how the nominal composition of cathode material influences the surface elemental and chemical structure as seen in the influence it exerts on the surface coating and the eventual electrochemical performance.

II. EXPERIMENTAL SECTION

II.A. Material Preparation. The pristine NMC532, NMC622, NMC811 and $LiNi_{0.8}Co_{0.15}Al_{0.05}O_2$ (Ni-rich NCA) powders were commercial cathode materials purchased from TODA America Inc. The $LiNi_{0.4}Co_{0.55}Al_{0.05}O_2$ (Co-rich NCA), $LiNi_{0.1}Co_{0.8}$ $Mn_{0.05}Al_{0.05}O_2$ (Co-rich NCMA) and $LiNi_{0.8}Co_{0.1}$ $Mn_{0.05}Al_{0.05}O_2$ (Ni-rich NCMA) were synthesized by the direct reaction of LiOH and a mixed-metal hydroxide with the correct stoichiometric ratio of cations, which is described in the previous study[28]. In the wet-coating process, the cathode powders were added into a pre-made solution of $Al(NO_3)_3{\cdot}9H_2O$

(Sigma Aldrich) and DI water (ratios between Al and pristine cathode powders were determined to produce a final Al_2O_3 ratio of 2 or 5 wt%), and was stirred at 400 rpm at room temperature for 6 h to make a good mixture. Then the temperature was raised to 80 ^oC to evaporate the water while stirring. The isolated mixture was then dried under vacuum for 4 h. The obtained as-coated powders were annealed at 400, or 800 ^oC for 8 h to assess the reactivity of the coating with the cathode.

II.B. Electrochemical Testing. Electrochemical half-cell tests were performed using 2032-type coin cells. The cathode electrode was prepared by laminating the powder on an Al foil current collectors with a slurry containing 90 wt% of the oxide powder, 5 wt% Super P carbon, and 5 wt% polyvinylidene difluoride (PVDF) binder in N-Methyl 2-Pyrrolidone (NMP). The electrolyte was a 1.2 M solution of $LiPF_6$ in a 3:7 mixture of ethylene carbonate (EC) and ethylmethyl carbonate (EMC). Celgard-2325 was used as the separator and the lithium metal plate was used as the anode. The cells were cycled between 3 and 4.5 V, first at the rate of C/10 for 4 cycles, then at C/3 for 50 cycles.

II.C. Structural Characterizations.

^{27}Al MAS NMR experiments were performed at two different fields; experiments to study influence of the bulk paramagnetic centers on the aluminum species at 7.02 T (300 MHz) on a Bruker Avance III HD spectrometer operating at a Larmor frequency of 78.204 MHz, and experiments to study diamagnetic species on 11.7 T (500 MHz) on Bruker Avance III spectrometer at a Larmor frequency of 130.25 MHz. For 7.02 T experiments, a rotor synchronized echo pulse sequence ($\pi/2$ - τ -π - acq.), where $\tau= 1/\nu_r$ (spinning frequency), was used to acquire the spectra with a 1.3 mm probe at a spinning speed of 67 kHz with a pulse width of 0.75 μs. For 11.7 T experiments, a rotor-synchronized echo pulse sequence with the pulse width of 1.5 μs was used to acquire the spectra with a 2.5 mm probe at a spinning speed of 30 kHz. Variable pulse delay times between 0.5 s to 15 s were used to the presence of diamagnetic aluminum species quantitatively. The spectra were referenced to 1M $Al(NO_3)_3$ aqueous solution at 0 ppm.

^{6}Li MAS-NMR experiments were performed at 7.02 T (300 MHz) on a Bruker Avance III HD spectrometer operating at a Larmor frequency of 44.21 MHz, using a 1.3 mm MAS probe. All spectra were acquired at 67 kHz with a rotor synchronized echo pulse sequence (90°-τ-180°-τ-acq), where $\tau= 1/\nu_r$. A $\pi/2$ pulse width of 1.5 μs was used with sufficiently long pulse recycle delays of 0.2 s. All spectra were collected at a constant temperature of 283 ± 0.1 K. All spectra were collected at a constant temperature of 283 K. The spectra were referenced to 1 M LiCl aqueous solution at 0 ppm. ^{7}Li MAS-NMR experiments were performed at 11.7 T on a Bruker Avance III HD spectrometer operating at a Larmor frequency of 44.21 MHz, using a 2.5 mm MAS probe. All spectra were acquired at 30 kHz with a rotor synchronized echo pulse sequence.

A $\pi/2$ pulse width of 2.5 μs was used with sufficiently long pulse recycle delays of 15 s. The spectra were referenced to 1 M LiCl aqueous solution at 0 ppm.

SEM images were taken using a Hitachi S-4700-II microscope in the Electron Microscopy Center of Argonne National Laboratory. The dry powders were directly sprayed onto the conductive carbon tape before imaging. Images were taken at 20 kV operating voltage.

TEM studies were performed at 200 kV on a JEOL 2100F in the Center for Nanoscale Materials of Argonne National Laboratory, equipped with Energy Dispersive Spectrometry (EDS) and the capability of nano-beam diffraction (NBD). For NBD, an area with the diameter of ~3 nm is used for each diffraction pattern. The NBD measurements are performed along line profiles in 1.5 nm steps toward the particle bulk. The images, diffraction patterns, and EDS results were taken using Gatan Digital Micrograph v2.01 (Gatan Inc.) and INCA (Oxford Instruments). The electron energy loss spectroscopy (EELS) was also measured using the same TEM with the energy resolution of ~0.2 eV.

High resolution synchrotron powder diffraction data were collected using beamline 11-BM-B with an average wavelength of 0.414 Å for all compounds. Samples were loaded in Kapton capillaries (0.9 mm diameter) and mounted on bases provided by the Advance Photon Source (APS), Argonne National Laboratory. Two platinum-striped collimating mirrors and a double-crystal Si(111) monochromator were used for the X-ray optics. The data points were collected at room temperature with a step size of 0.001° 2θ and scan speed of 0.01 °/sec. Data were collected while continually scanning the diffractometer 2θ arm. High resolution and short collection time were obtained by using a unique 12-element Si (111) crystal analyzer/detector. Rietveld refinements were performed using TOPAS[30].

II.D. DFT Calculations. DFT calculations were carried out by the spin-polarized DFT as implemented in the Vienna Ab Initio Simulation Package (VASP)[31-32]. The exchange-correlation potentials are treated by the generalized gradient approximation (GGA) parametrized by Perdew, Burke, and Ernzerholf (PBE)[33]. The interaction between valence electrons and ion cores is described by the projected augmented wave (PAW) method[34]. Furthermore, the GGA+U scheme is used for applying the on-site correlation effects among 3d electrons of the transition metals (TM), where the parameter of (U-J) is set to 5.96eV, 5.00eV, and 4.84eV for Ni, Co, and Mn respectively[35]. The wave functions were expanded in the plane wave basis up to a kinetic energy of 500eV. All the ions were allowed to be relaxed until the total energy differences were no more than 0.003eV. After geometry optimization within the DFT+U framework, electronic relaxation was performed using a single point calculation with the hybrid functional HSE06[36], to determine the surface energy at that level of theory. The detailed results and discussion of the DFT results can be found in the Supporting Information (SI).

III. RESULTS AND DISCUSSIONS

III.A. Surface and Bulk Characterization of Pristine Cathodes. Since the interaction between the coating and the cathode material is greatly influenced by the nature of the surface and bulk of pristine cathode materials, the initial characterization studies were focused on pristine NMC particles. The pristine NMC532, 622 and 811 powders have similar particle size and morphologies with good crystallinity, as shown in the SEM and TEM images in Figure S1 in the SI. EDS and NBD equipped TEM was used to determine the surface chemistry and lattice structure of the pristine samples. The smallest aperture was selected for the EDS and NBD line profiling to reduce the beam diameter to ~3 nm, which allowed us to characterize the chemical compositions and lattice parameters in the small local regions from the surface and edge to the bulk of the oxide. Figures 1a-1c show the EDS line profiling results of the pristine NMC particles, scanning from the surface to the bulk. The circle and arrow in each TEM image in Figures 1a-1c correspond to the initial beam spot and the scanning direction for the EDS profiling. Co-rich surfaces are observed in all the pristine particles, which may result from the thermal history of the oxide particles. Similar Co segregations on the pristine NMC surface have been reported on $LiNi_{0.33}Mn_{0.33}Co_{0.33}O_2$ (NMC111) and $LiNi_{0.4}Mn_{0.4}Co_{0.2}O_2$ (NMC442) in a previous TEM study with composition and facet dependence [37]. However, to our best knowledge, the surface Co segregation on the Ni-rich NMC532, 622 and 811 has not been reported before. Due to the lack of –control with regard to crystallite faceting with the commercial NMC particles, the effect of facet on surface segregation will not be discussed in this paper. The Co segregation could have a big influence on the Al insertion process after annealing the coated NMC particles, which will be discussed in a later session. The lattice spacing evolution measured from the NBD line profiling shows that the lattice parameters of the pristine particles are the same both in the bulk and on the surface, indicating a homogeneous lattice structure for the pristine samples (see Figures 1d-1f).

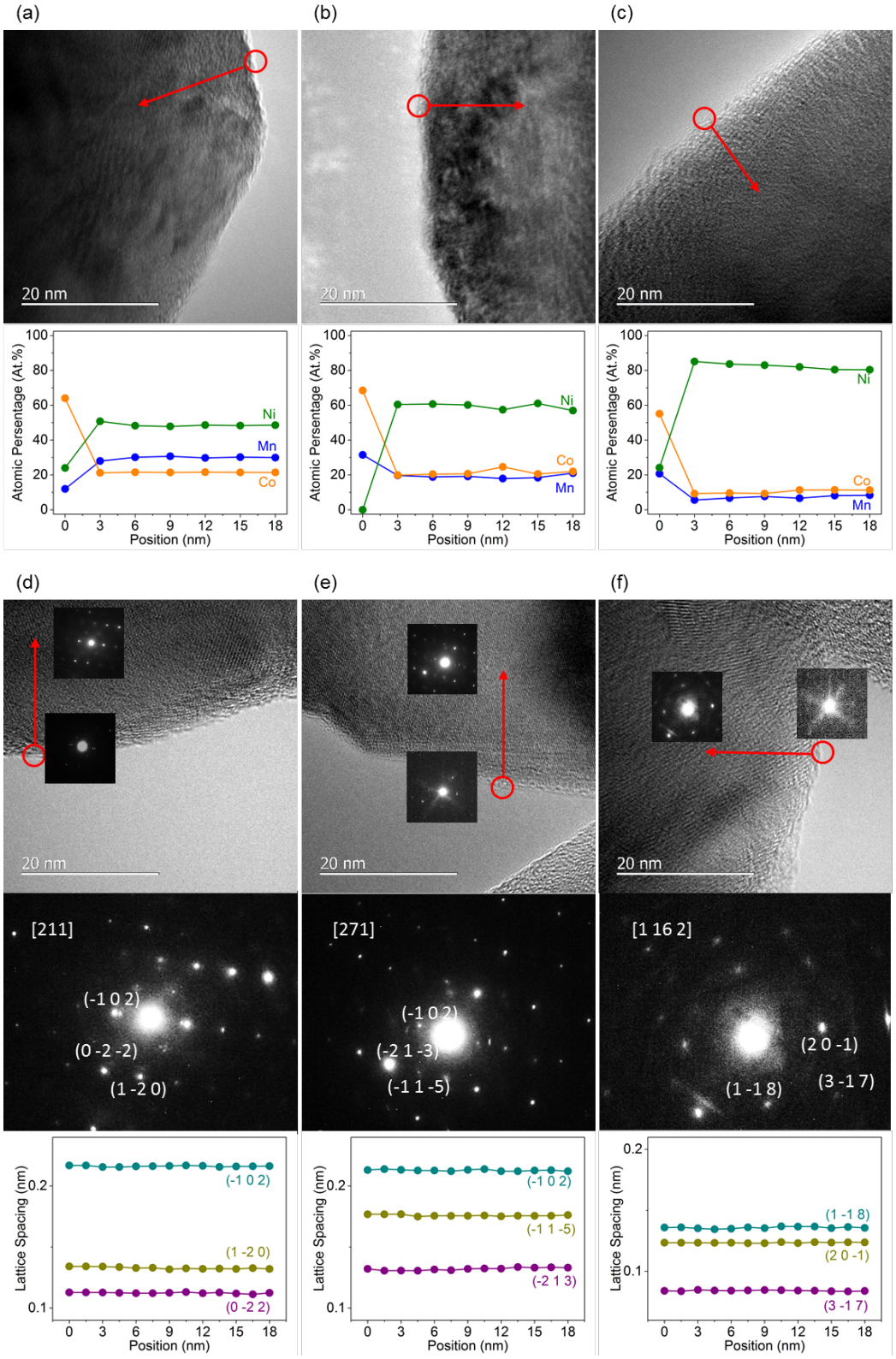

Figure 1. EDS line profiling and the relative metal composition results on (a) pristine NMC532, (b) pristine NMC622, and (c) pristine NMC811. NBD line profiling, diffraction patterning and the lattice

spacing results on (d) pristine NMC532, (e) pristine NMC622, and (f) pristine NMC811. The TEM images in each panel showed the corresponding particles for EDS or NBD characterization. The red circle in each TEM image represent the start point and the beam size, and the red arrow represents the line scan direction.

To further study the bulk lithium local environments and surface species on pristine particles, particularly the surface lithium species which cannot be measured accurately by EDS, ^{6}Li or ^{7}Li MAS NMR experiments have been performed on pristine samples. Figure 2a shows natural abundance ^{6}Li MAS NMR of pristine NCM cathode with varying transition metal compositions. For all the samples a major broad peak around 550-600 ppm is observed. This large shift is assigned to the hyperfine interaction between lithium nuclear spin and the unpaired electrons of paramagnetic Ni^{2+}/ Ni^{3+},Mn^{4+} ions (Co^{3+} being diamagnetic does not contribute to hyperfine shift) and can be assigned to Li ions in lithium layers.[38-39] The presence of a broad featureless peak for the samples suggests a less ordered, solid-solution-like bulk structure for all the NMC compositions. One of the major differences observed with ^{6}Li MAS NMR for the bulk local structure with varying transition metal composition is the peak width and slight shift in the observed peak positions. The NMC811 sample shows more local order, with relatively narrow line width distributed between 200 to 850 ppm due to the presence of high concentration of Ni^{3+}. For NMC532 and 622 the observed peaks are wider and distributed over to both higher (1000 ppm) and lower (50 ppm) frequencies due to the presence of higher paramagnetic Mn^{4+} and diamagnetic Co^{3+} content, respectively as well as presence of a mixture of Ni^{2+} and Ni^{3+} creating a wider distributions of local coordination for lithium. Another difference between the different compositions is the presence of a second resonance observed for NMC532 sample as a small shoulder at around 1300 ppm. This minor peak can be assigned as Li in transition metal layers with Ni and Mn in 1st and 2nd coordination shell as a result of mixing of lithium with similar size Ni^{2+}. However for stoichiometric NMC, especially for Ni-rich compositions, ^{6}Li MAS NMR cannot fully capture the Li/Ni exchange rate. Therefore, HRXRD was used to calculate the Li/Ni exchange in NMC622 and NMC811compositions. As shown in Table S1 in the SI, the Li/Ni exchange rate in pristine NMC622 and NMC811 are 2.66% and 1.12%, respectively.

In order to study the presence and quantify the surface/diamagnetic Li species among the pristine NMC samples with varying transition metal composition, ^{7}Li MAS NMR experiments were performed and the mass-normalized results are shown in Figure 2b. Here the bulk Li peak has been removed by subtracting the fast-relax signals during the data processing to only show the surface Li peaks. From Figure 2b we can see that from NMC532 to NMC811, the decreasing Mn contents and the increasing Ni contents lead to more surface and/or diamagnetic lithium environments. The nature of these environments can be a segregated $LiCoO_2$ phase or surface Li_2CO_3 and Li_2O. LiOH is not considered to be present as

the ^{1}H NMR experiments on the same samples (data not shown) do not show significant proton environments.

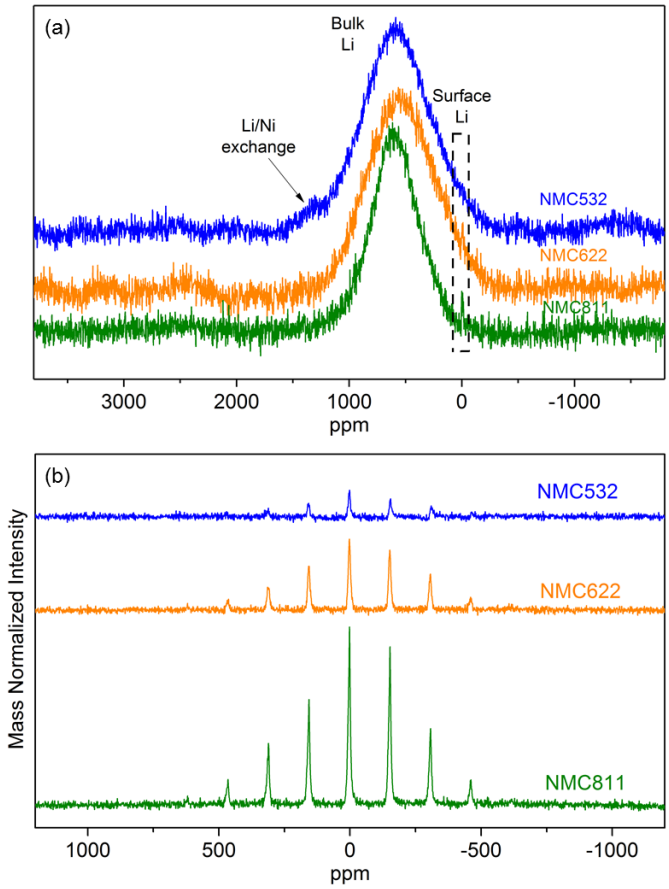

Figure 2. (a) ^{6}Li MAS NMR spectra of pristine NMC532, NMC622 and NMC811 with signals from both the bulk and the surface Li, measured at 7.02 T with the spinning speed of 67 kHz. The spectra were normalized to the main peak at ~500 ppm. (b) Mass-normalized ^{7}Li MAS NMR spectra of pristine NMC532, NMC622 and NMC811 measured at 11.7 T with the spinning speed of 30 kHz, where the bulk Li peaks have been removed during the data processing.

III.B. Surface and Bulk Characterization of Aluminum coated NMC cathodes.

The effect of transition metal composition on the coating processes, including aspects such as chemical and structural change of coating, interfacial layers, and the diffusion of Al into the bulk of the oxide, were studied on aluminum coated NMC532, 622 and 811 cathodes. The initial studies focus was on 2 wt% Al_2O_3 coatings as this level was found to be amenable to further characterization of the Al(III) containing species, helped to facilitate the characterizations on coating compositions, local structures, and

morphology changes. The coated samples were annealed at 400 and 800 ^{o}C in air for 8 h to form a denser layer on the cathode particles.

In one of our previous studies, using the ^{27}Al MAS NMR methods, we showed that with increasing annealing temperature applied onto a 2% Al_2O_3-coated NMC532, the phase γ-$LiAlO_2$ was formed when the heating temperature is above 600 ^{o}C [29], due to the interfacial reaction between alumina coatings and surface Li species on NMC particles. In this study, for both 2% Al_2O_3-coated NMC622 and 811 particles, 4-coordinate ^{27}Al peaks at ~69 ppm can be found in the NMR spectra after heating at 800 ^{o}C (see Figure 3b), which represents the formation of γ-$LiAlO_2$ phase, similar to our previous finding on Al_2O_3-coated NMC532. ^{27}Al MAS NMR data also shows a broad and distorted peak at ~15 ppm, which can be assigned to the presence of 6-coordinate Al_2O_3 and/or α-$LiAlO_2$. In addition, coated and 800 ^{o}C-annealed NMC811 and 622 have a broad peak centered around -1000 ppm (Figure 3a). This large shift is due to a hyperfine interaction and suggests the presence of paramagnetic lattice aluminum resulting from diffusion of aluminum cations from the surface to the bulk at high temperature[28], which is missing in Al_2O_3-coated NMC532. High-resolution ^{27}Al MAS NMR experiments were performed on higher aluminum content coated samples to further study this potential Al-cation diffusion into the bulk and the nature of these aluminum environments in NMC622 and 811 and the data will be discussed in a later session of this paper. Another significant difference observed with different cathode compositions is the relative intensity difference between the 4-coordinate (γ-$LiAlO_2$) peak and 6-coordinate (Al_2O_3 and/or α-$LiAlO_2$) peak as seen with ^{27}Al MAS NMR (Figure 3b). With NMC811 composition this ratio is the lowest, indicating less γ-$LiAlO_2$ formation after high-temperature annealing, despite the high initial surface Li contents on the pristine NMC811 (Figure 2b). An accurate analysis on the quantification of interfacial species is obtained by repeating experiments with longer pulse delay times providing full relaxation of aluminum species. The results of long-pulse-delay (15 s) experiments in Figure S6a demonstrate stronger 4-coordinate signals on 2% Al_2O_3-coated NMC622 and NMC811 compared with the short-pulse-delay (0.5 s) results, indicating the 4-coordinate γ-$LiAlO_2$ phase on NMC622 and NMC811 has longer relaxation time in NMR measurements. However, even in the long-pulse-delay NMR measurements, the ratio between 4- and 6-coordinate signals still decrease from NMC532 to NMC811 (Figure S6). These significant compositional differences of the interface can be due to the surface segregation and/or the diffusion of surface alumina into the oxide lattice mentioned above. In order to understand the interface formation and the distribution of different $LiAlO_2$ phases on the surface, DFT calculation has been performed. The energy calculations suggest that a few layers of α-$LiAlO_2$ (with 6-coordinate Al environment) may form as a buffer between the bulk NMC and the surface γ-$LiAlO_2$ (see Figure S7 in the SI) to accommodate the large lattice mismatch between them. These calculation results overlap with diamagnetic (surface) peaks observed with ^{27}Al NMR and the relaxation time differences between 4- and

6-coordinate signals, the former having a longer relaxation due to being more isolated and at a greater distance from the paramagnetic bulk, the presence of which reduces the relaxation rates [40].

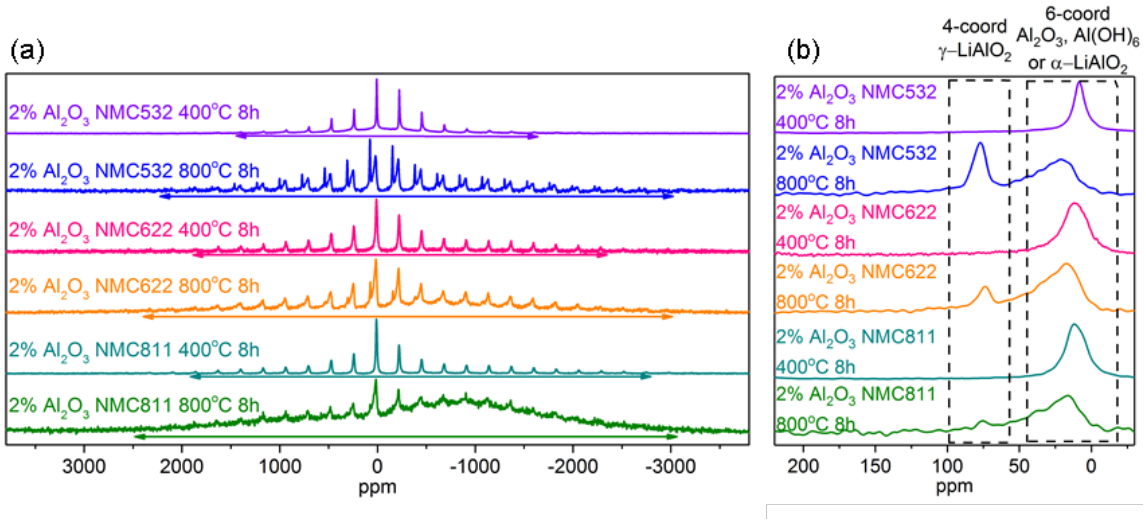

Figure 3. (a) ^{27}Al MAS NMR data for 2% Al_2O_3-coated NMC532, NMC622 and NMC811 samples annealed at 400 or 800 °C for 8h taken at 11.7 T with the spinning speed of 30 kHz. (b) The zoom-in plot of the diamagnetic region showing only the main ^{27}Al peaks without spinning sidebands. The spectra were normalized to the main peak at ~0 ppm. The pulse delay time was 0.5 s.

An increase in the span of spinning sideband envelope on ^{27}Al MAS NMR of Al_2O_3-coated NMC532 after annealing at a higher temperature can also be observed (Figure 3a), consistent with our previous work[29]. This wide sideband envelope represents a stronger interaction between surface Al coatings and bulk paramagnetic metal centers, implying a closer and smoother surface coating formed with high-temperature treatment. A similar but less pronounced trend can be found for Al_2O_3-coated NMC622 and NMC811 in this work (Figure 3a). One possible explanation for the reduced sideband intensity and overall interfacial aluminum peak intensity in Al_2O_3-coated NMC622 and 811 compared to 532 can be the partial aluminum insertion into the lattice with lower Mn content. The formation of a more uniform and more closely attached coating on the surface after high-temperature annealing can be further confirmed by the SEM images shown in Figure S3. The as-coated NMC particles in Figure S3 have a loose amorphous coating covering the whole secondary particle, in spite of the transition metal composition. After being annealed at 400 °C, the coating layer becomes denser but still maintains morphological aspects of its initial amorphous nature, whereas a much smoother and hard-shell-like coating forms on the surface with increasing to temperature to 800°C. These trends are consistent with the NMR observations in Figure 3a

and are similar to our previous observation on NMC532 [29], demonstrating the significant influence of annealing temperature on the surface coating morphology on different NMC particles.

To further study the diffusion of aluminum into the lattice and its local environment in Al_2O_3-coated NMC622 and NMC811 shown in Figure 3a, we increased the loading of Al_2O_3 from 2 to 5 wt% in order to get stronger signals in NMR measurements. Figure 4a shows the ^{27}Al MAS NMR data performed at a lower magnetic field (7.04 T) with a high spinning speed (67 kHz) for 5% Al_2O_3-coated NMC622 and NMC811 annealed at 800 ^{o}C. Ni- and Co-rich NCA and Al-doped NCM samples were synthesized as model systems and studied with ^{27}Al MAS NMR for comparison. The high-resolution NMR data in Figure 4a reveals that on Al_2O_3-coated NMC622, after annealing at 800 ^{o}C, at least three broad peaks can be observed at around -200, -400 and -600 ppm, while for Al_2O_3-coated NMC811, more pronounced peaks can be observed in the same region. These peaks represent the lattice Al within transition metal layers, proving that surface alumina inserts into the layered oxides NMC622 and NMC811 after annealing at 800 ^{o}C. The three peaks at -200, -400 and -600 ppm can be assigned as Al cations surrounded within the transition metal layer by one Ni and five Co cations, designated Al-1Ni5Co, as well as the more Ni-rich environments Al-2Ni4Co, and Al-3Ni3Co environments, consistent with our previous studies on NCA[28], which are all Co-rich Al(III) environments within this Ni rich composition. The presence of lattice Al in a Co-rich rather than Ni-rich environment in Ni-rich materials such as NMC811 and 622 is unexpected, suggesting surface Co segregation, which will be discussed in a later session. The fact that the lattice Al peaks on Al_2O_3-coated NMC811 are much higher and sharper compared to that on Al_2O_3-coated NMC622 implies that the diffusion of surface Al into the bulk of NMC811 is much favorable and pronounced than that in NMC622. The effect of aluminum substitution into the lattice on bulk lithium local environment is also studied by ^{6}Li MAS NMR. As seen in Figure 4b, the bulk Li environment (represented by the main peak ~500 ppm) has a large change in 5% Al_2O_3-coated NMC811 annealed at 800 ^{o}C compared to the pristine NMC811. In contrast, the differences in the ^{6}Li MAS NMR spectra of the 5% Al_2O_3-coated NMC622 and pristine NMC622 are very limited. This again shows that after annealing the Al_2O_3-coating on NMC811, surface Al(III) inserts into the bulk of the particle, which clearly changes the chemical environment of bulk Li atoms. On NMC622 the insertion of surface Al(III) into the bulk after annealing is much weaker. This favorable Al cation diffusion observed on Al_2O_3-coated NMC811 after high-temperature annealing is correlated with low Mn content and/or high Co content due to surface segregation. Our previous work reported the diffusion of an alumina surface coating into the bulk of LCO after annealing at relatively low temperatures, while the similar insertion was prevented on NMC532 even after annealing at relatively high temperatures, which has been thought to be due to the strong incompatibility between Al and Mn cations in layered oxide environments when exposed to higher annealing temperatures[29]. DFT calculation in this work confirm that the adjacent pairs of Al and Mn

cations in the transition metal layer of NMC structures are thermodynamically unfavorable (Figures S8d and S8e). In contrast, it is thermodynamically favorable to substitute the surface Al into the position surrounded by only Ni and Co cations in the transition metal layer (Figure S8c). Such a blocking effect of Mn cations to the Al insertion process can explain the compositional dependence of Al coating-to-dopant transition observed in this work. In the case of NMC811 (which has 10% Mn in its transition metal layers), using a random transition metal distribution, the probability of a Mn-free second coordination sphere within the honeycomb ordering of these phases is: $p_{\text{Mn-free}} = 0.9^7 \approx 0.48$, which is much higher than that in NMC622 ($p_{\text{Mn-free}} \approx 0.21$) and in NMC532 ($p_{\text{Mn-free}} \approx 0.08$). Therefore, the insertion of surface aluminum cations into the bulk and the presence of lattice aluminum in transition metal layer is more favorable for a Ni-rich and Mn-deficient material such as NMC811.

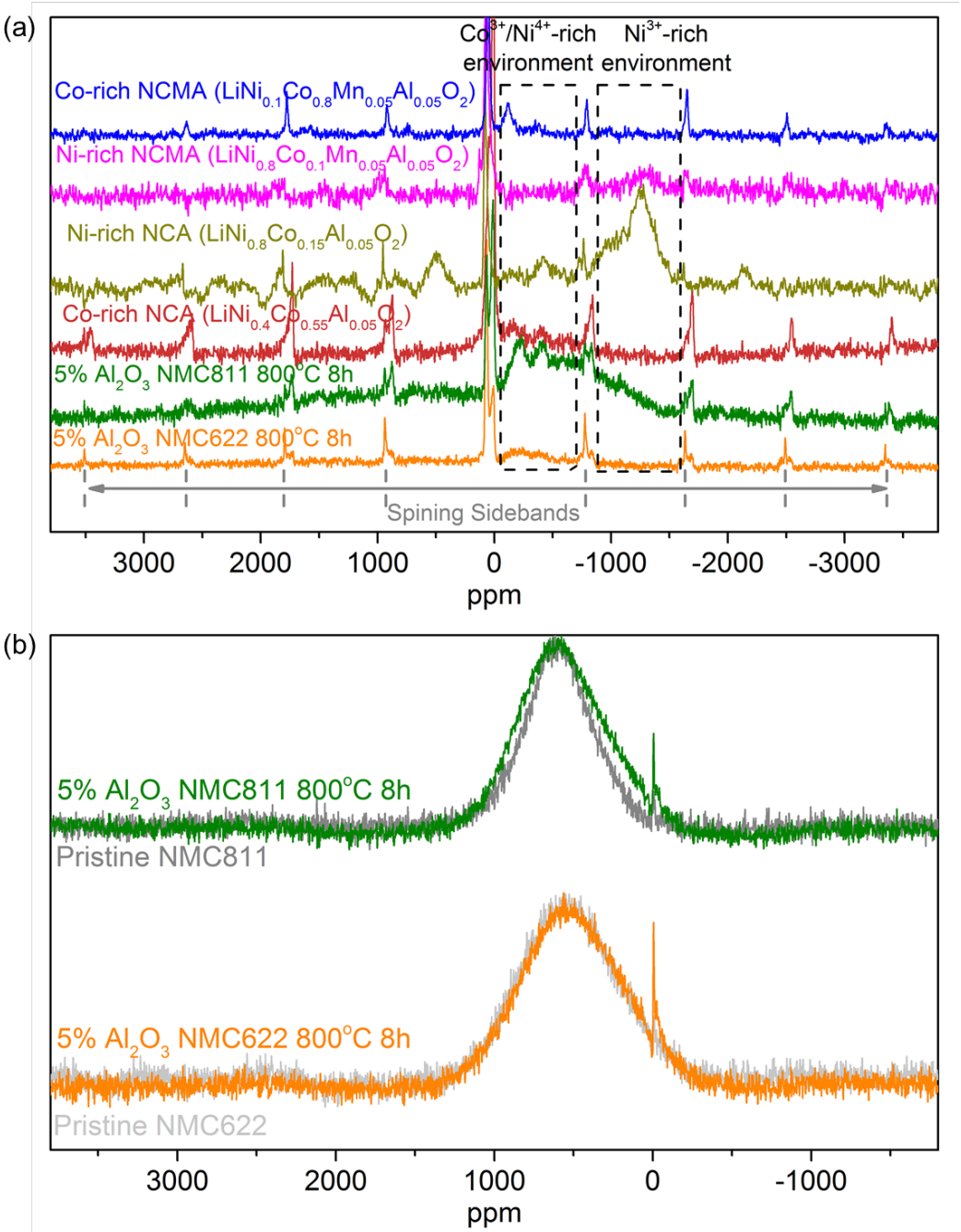

Figure 4. (a) ^{27}Al MAS NMR spectra of 5% Al_2O_3-coated NMC622 and NMC811 annealed at 800 ^{o}C for 8h, compared to Co-rich NCA, Ni-rich NCA, Ni-rich NCMA and Co-rich NCMA measured at 7.02 T with the spinning speed of 67 kHz. The spectra were normalized to the main peak at 0 ppm. The positions of spinning sidebands are marked by the grey dash lines at the bottom. (b) ^{6}Li MAS NMR spectra of 5% Al_2O_3-coated NMC622 and NMC811 annealed at 800 ^{o}C for 8h, compared to pristine NMC622 and NMC811, all measured at 7.02 T with the spinning speed of 67 kHz. The spectra were normalized to the main peak at ~500 ppm. The pulse delay time was 0.5 s.

As mentioned above, the presence of lattice Al in a Co-rich environment (see Figure 4a) in Ni-rich materials such as Al-inserted NMC811 and 622 is unexpected. In fact, in the Ni-rich layered oxides with Al substitution, such as in the Ni-rich NCA ($LiNi_{0.8}Co_{0.15}Al_{0.05}O_2$) or Ni-rich NCMA ($LiNi_{0.8}Co_{0.1}Mn_{0.05}Al_{0.05}O_2$), the lattice Al tends to be surrounded by mainly 5 or 6 paramagnetic Ni^{3+} metal centers, giving ^{27}Al NMR resonances at around -1300 ppm, as shown in Figure 4a. The fact that the inserted bulk Al environments in NMC811 and 622 are similar to Co-rich NCA ($LiNi_{0.4}Co_{0.55}Al_{0.05}O_2$) and Co-rich NCMA ($LiNi_{0.1}Co_{0.8}Mn_{0.05}Al_{0.05}O_2$) suggests either there is a strong surface Co segregation, or there are other diamagnetic metal centers such as Ni^{4+} formed during the coating and annealing process. The first hypothesis could be supported by the EDS results in Figures 1a-1c, where surface Co segregations are observed on all the pristine NMC particles. EDS profiling results on 5% Al_2O_3-coated NMC particles annealed at 800 ^{o}C shown in Figures 5a-5c demonstrate that the coated samples also have surface Co segregations even after the coating and annealing process. This non-homogenous distribution of transition metals with a larger ratio of Co near the surface of NMC particles results in aluminum environments surrounded by diamagnetic Co^{3+} rather than paramagnetic Ni^{3+} after diffusing from surface coating layers into the bulk during the high-temperature annealing. As seen in Figure 4a, the differences observed in ^{27}Al NMR resonances reflects the importance of direct Al doping versus surface diffusing on the aluminum coordination in the structure. When directly doping the Al into the bulk oxides, similar to the NCA particles, the Al precursor is evenly distributed in the bulk of layered oxides. Therefore the substituted lattice Al cations show a different environment between Ni-rich and Co-rich NCA (Figure 4a), which is determined by the major transition metals content in the bulk. However, when the surface Al cations diffuse into the bulk with the increasing annealing temperature, since it is a surface process, the Al cations within the coating layers will be greatly influenced by the surface segregation layer rather than the average bulk concentration of transition metals. Therefore, this surface segregation can be used to control the formation of preferential Al substitution in the lattice and change the Al local environment by annealing a coated material at high temperature rather than directly doping Al into the bulk by adding Al into the precursors during oxides synthesis, which may lead to different impacts on the electrochemical performances. Additionally, the surface segregation of Co may also facilitate the Al diffusion process by reducing the Mn content near the surface and/or by reducing the energy penalty of the Mn-Al incompatibility. As shown by the DFT results in Figure S8d, when surrounded by 3 Mn and 3 Co, the thermodynamic energy penalty for Al insertion is only slightly higher than 0 (0.03 eV). In contrast, when surrounded by 3 Mn and 3 Ni, the energy penalty for Al insertion is much higher (0.95 eV, Figure S8e). Therefore, the surface Co segregation may reduce the blocking effect of Mn on the Al insertion.

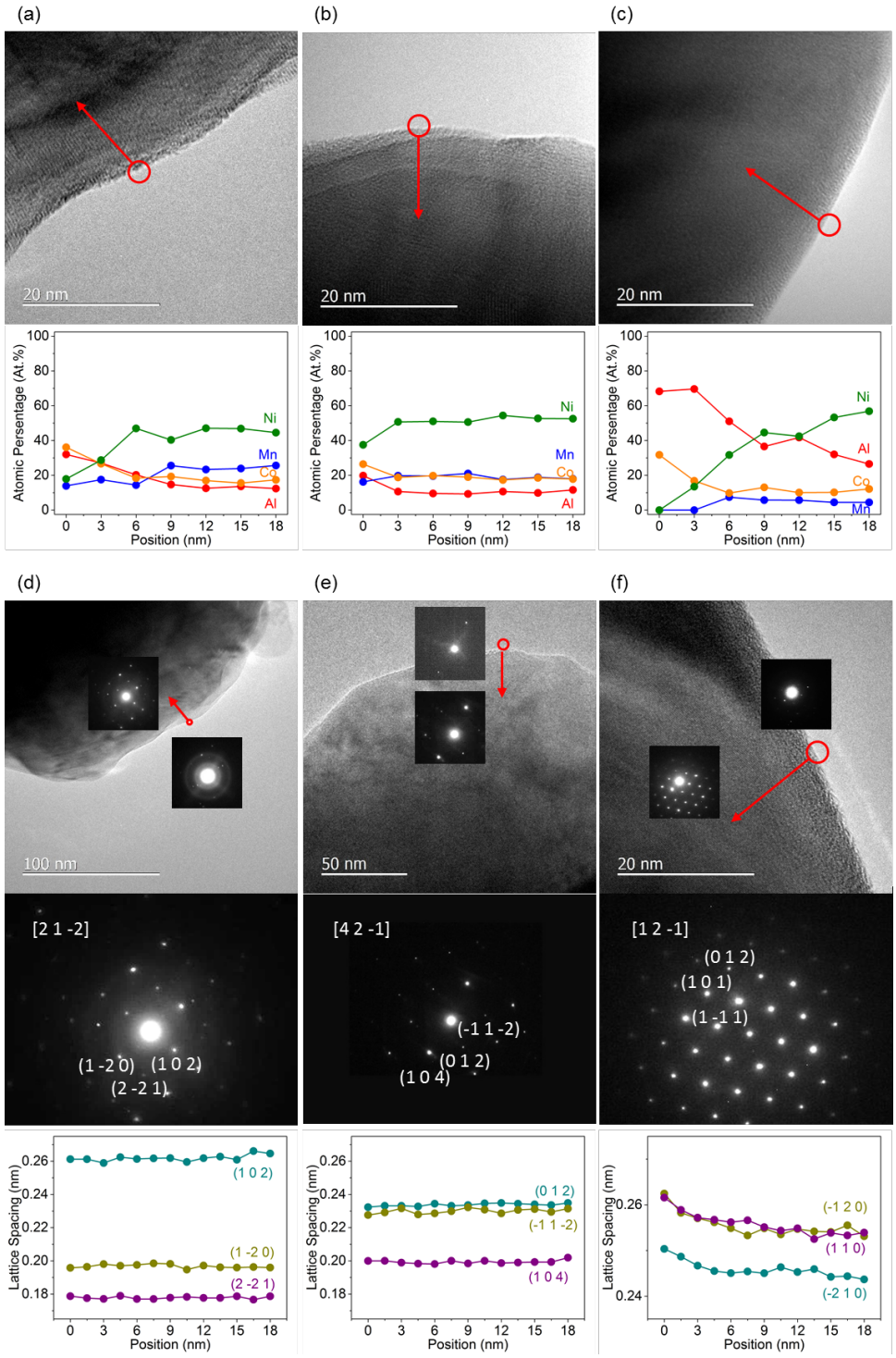

Figure 5. EDS line profiling and the relative metal composition results on (a) 5% Al_2O_3-coated NMC532, (b) 5% Al_2O_3-coated NMC622, and (c) 5% Al_2O_3-coated NMC811, all annealed at 800 ^{o}C for 8h. NBD line profiling, diffraction patterning and the lattice spacing results on (d) 5% Al_2O_3-coated NMC532, (e) 5% Al_2O_3-coated NMC622, and (f) 5% Al_2O_3-coated NMC811, all annealed at 800 ^{o}C for 8h. The TEM images in each panel show the corresponding particles for EDS or NBD characterization.

The red circle in each TEM image represent the start point and the beam size, and the red arrow represents the line scan direction.

The second hypothesis, that the surface paramagnetic Ni^{2+}/Ni^{3+} is being oxidized to diamagnetic Ni^{4+}, could be related to the Li consumption observed during the Al insertion process. When annealing at high temperature in air, the surface alumina coating may react with the Li in the bulk, causing the oxidation of Ni^{3+} in the near-surface layers. One of the potential schematic reaction formula could be: $x\mathrm{Al_2O_3} + \frac{x}{2}\mathrm{O_2} + \mathrm{LiNi^{3+}O_2} \xrightarrow{\Delta} 2x\mathrm{LiAlO_2} + \mathrm{Li_{1-2x}Ni^{3+}_{1-2x}Ni^{4+}_{2x}O_2}$. To test this hypothesis, we measured EELS of Ni $L_{2,3}$ edges on both pristine and 5% Al_2O_3-coated NMC particles, as shown in Figure S4. For the EELS collected from the surface regions of pristine samples, a slight voltage shift of ~1 eV can be observed compared with the bulk EELS results, implying a potential reduction of Ni on the surface. The similar surface metal reduction has been observed previously on NMC particles[41]. In comparison, the 5% Al_2O_3-coated NMC particles, the Ni L_3 peak shifts in the surface regions compared with the bulk are less pronounced, indicating the wet coating of Al_2O_3 could make the surface Ni less reduced due to the surface Li consumption. Nevertheless, there is no clear evidence of further Ni cation oxidation to Ni^{4+} on the surface of 5% Al_2O_3-coated NMC811 or NMC622 particles. Therefore, smaller hyperfine shift for ^{27}Al resonances observed in Figure 4a is more likely caused by the surface Co^{3+} segregation rather than the existence of Ni^{4+}.

The presence of aluminum diffusion into the bulk NMC622 and 811 can be further studied via NBD line profiling from the surface to the bulk of Al_2O_3-coated NMC particles. The NBD results in Figure 5f shows that the surface lattices of 5% Al_2O_3-coated NMC811, although are continuous from the bulk layered structures, have ~3% larger lattice parameters due to the high content of bigger Al^{3+} cations near the surface layers. On the contrary, the surface lattice spacing of 5% Al_2O_3-coated NMC622 and NMC532 is almost the same as that in the bulk (Figures 5d and 5e), implying the structure of layered oxide is not significantly changed at the surface and the Al_2O_3 has not diffused (or only diffused a short distance) into the bulk of NMC532 or NMC622 after the annealing process. The above observations indicate the diffusion of surface Al_2O_3 into the NMC811 is much easier than into NMC622 or 532, which is consistent with the NMR results in Figure 4a. In addition, the EDS line profiling in Figures 5a and 5b show that the Al concentration is high when detecting the edge of the particle, representing a thin Al-rich layer covered the whole particle of NMC532 and NMC622. In comparison, for 5% Al_2O_3-coated NMC811, Figure 5c demonstrates that its surface Al content increases from the surface to the bulk compared to those for NMC532 and NMC622. This again, shows that NMC811 has a higher tendency for aluminum diffusion into the bulk after high-temperature annealing.

The lattice structure evolution after the diffusion of surface Al into the bulk of NMC811 and 622 was further investigated by HRXRD, as shown in Figure S9. The HRXRD refinement results in Table S1 demonstrate that compared with the pristine sample, the average lattice parameters (a and c) of the 5% Al_2O_3-coated NMC811 increased by 0.21% and 0.23% respectively after annealing at 800 ^oC. While in the case of NMC622, the changes of average lattice parameters (a and c) in coated samples are only 0.16% and 0.09%, respectively, which are much smaller compared with the changes in coated NMC811. This trend is consistent with the NBD results in Figure 5 showing that the surface lattice of NMC811 expanded significantly after the Al insertion process, which is not observed in NMC622, indicating the Al diffusion is a more severe process than in NMC811. Meanwhile, an obvious asymmetric distortion can be observed in the fitting of 5% Al_2O_3-coated NMC811 HRXRD data, as shown in Figure S9c, suggesting the presence of a large amount of stacking faults caused by Al insertion process. Further experiments are required to distinguish whether these stacking faults originate from the diffused Al or the substituted transition metals. Due to this big distortion, it is hard to accurately determine the Al(III) occupancy in transition metal layers in 5% Al_2O_3-coated NMC811 using HRXRD refinement in this paper. However, an estimated lattice Al occupancy of ~2.2% in 5% Al_2O_3-coated NMC811 can be obtained, which is larger than that calculated for 5% Al_2O_3-coated NMC622 (1.5%). This confirms that more Al cations diffused into NMC811 than NMC622 after the same annealing condition. In addition, several non-NMC peaks can be observed in the 5% Al_2O_3-coated samples in Figure S9b, which actually represents the γ-$LiAlO_2$ formed after the coating and annealing processes, consistent with the ^{27}Al NMR results in Figure 3b. Figure S9b also shows that the amount of γ-$LiAlO_2$ on coated NMC622 is much higher than that on coated NMC811, which is consistent with the long pulse delay ^{27}Al NMR results in Figure S6d.

The facilitated aluminum insertion on NMC811 leads to obvious morphology difference in SEM observations. Figure 6 shows the SEM images of Al_2O_3-coated NMC particles with various Al_2O_3 loadings from 0.5 to 5 wt%. With very low Al_2O_3 loading of 0.5 wt%, all the coated NMC particles demonstrate very smooth surface after annealing at 800 ^oC, indicating that all the surface Al either forms a smooth coating layer on the surface or diffuses into the bulk. When increasing the initial Al_2O_3 loading to 1, 2 and 5 wt%, on coated NMC532 and NMC622 some small particles start to emerge, while on coated NMC811 the particle always remains smooth. The small particles on Al_2O_3-coated NMC532 annealed at 800 ^oC have been reported in our previous paper, which were attributed to the excess Al_2O_3 aggregated on the surface during high-temperature treatment[29]. The presence of lower surface lithium content and the high aluminum diffusion barrier in NMC532 restrict the formation of $LiAlO_2$ and formation of lattice Al(III) during heat treatments, forming aggregated alumina on the surface. As for NMC622 with more surface Li species (see Figure 2b) and a small amount of Al diffusion into its bulk, after the high-temperature annealing, there is less Al_2O_3 left on the surface and aggregate into particles.

Therefore, the size of the scattered particles on NMC622 is smaller than that on NMC532 under the same Al loadings. In the case of NMC811, the NMR and NBD results have demonstrated that surface Al_2O_3 can easily diffuse into the bulk after annealing, and there is much more of the initial surface Li species on NCM811 (see Figure 2b). As a result, there is no scattered Al_2O_3 particle left on the surface even under very high Al_2O_3 loadings, as observed in Figure 6. A scheme of the coating morphology evolution can be found in Figure 7. The TEM images and EDS results on 5% Al_2O_3-coated NMC particles in Figure S5 confirmed that the surface smooth coating on all NMC particles are Al-containing crystalline layers, while the excess small particles on Al_2O_3-coated NMC532 or 622 are mainly the extra Al_2O_3 that failed to merge into the smooth surface coating. ^{27}Al NMR measurements with long pulse delay (15 s) are also used to study the evolution of surface species when increasing the Al_2O_3 loadings. As shown in Figure S6, for all the NMC materials, increasing the Al_2O_3 loadings from 2% to 5% dramatically increases the ratios between surface 4-coordinate and 6-coordinate signals, indicating that the extra Al_2O_3 added onto the NMC particles prefer forming $LiAlO_2$ surface layers, rather than staying in the form of Al_2O_3. As seen in Figure S6d this ratio is increased from NMC532 to NMC622, due to the more abundant surface Li species on NMC622; and then decrease from NMC622 to NMC811, as NMC811 has less surface aluminum species and more lattice aluminum due to a large amount of Al insertion.

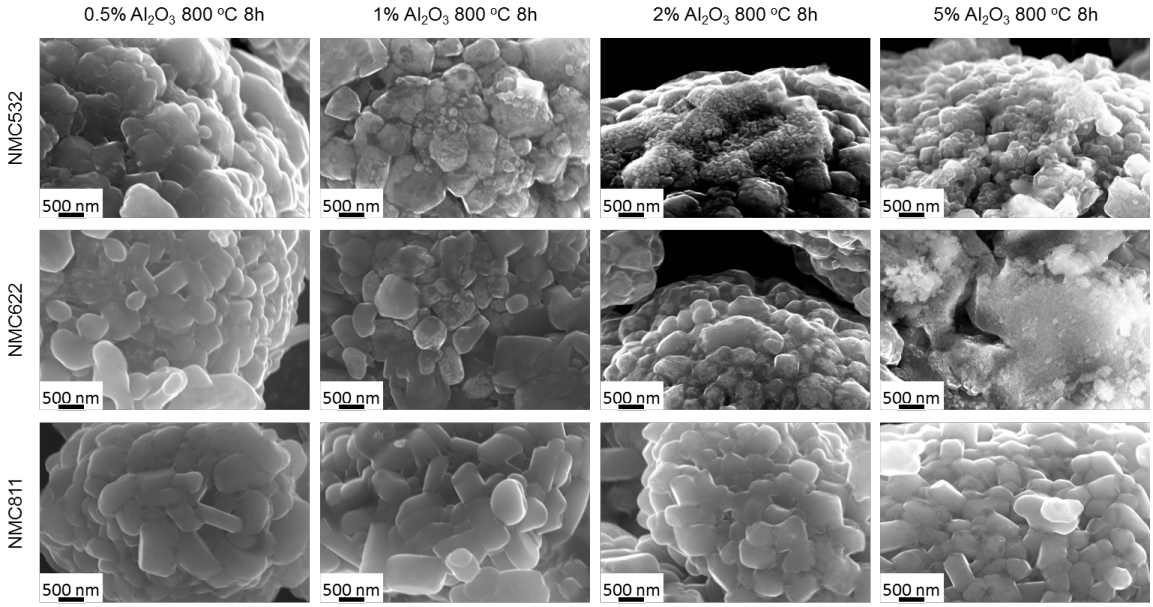

Figure 6. SEM images of Al_2O_3-coated NMC532, NMC622 and NMC811, with Al_2O_3 loading of 0.5, 1, 2 and 5 wt%. All samples were annealed at 800 ^{o}C for 8 h.

Combination of these detailed surface and bulk characterization studies reveals the importance of cathode surface compositions, coating contents, and annealing temperatures on surface morphologies, interfacial compositions, and changes in bulk structure. The evolution of surface, interface, and aluminum local coordination environments in the coated samples are summarized with a scheme in Figure 7.

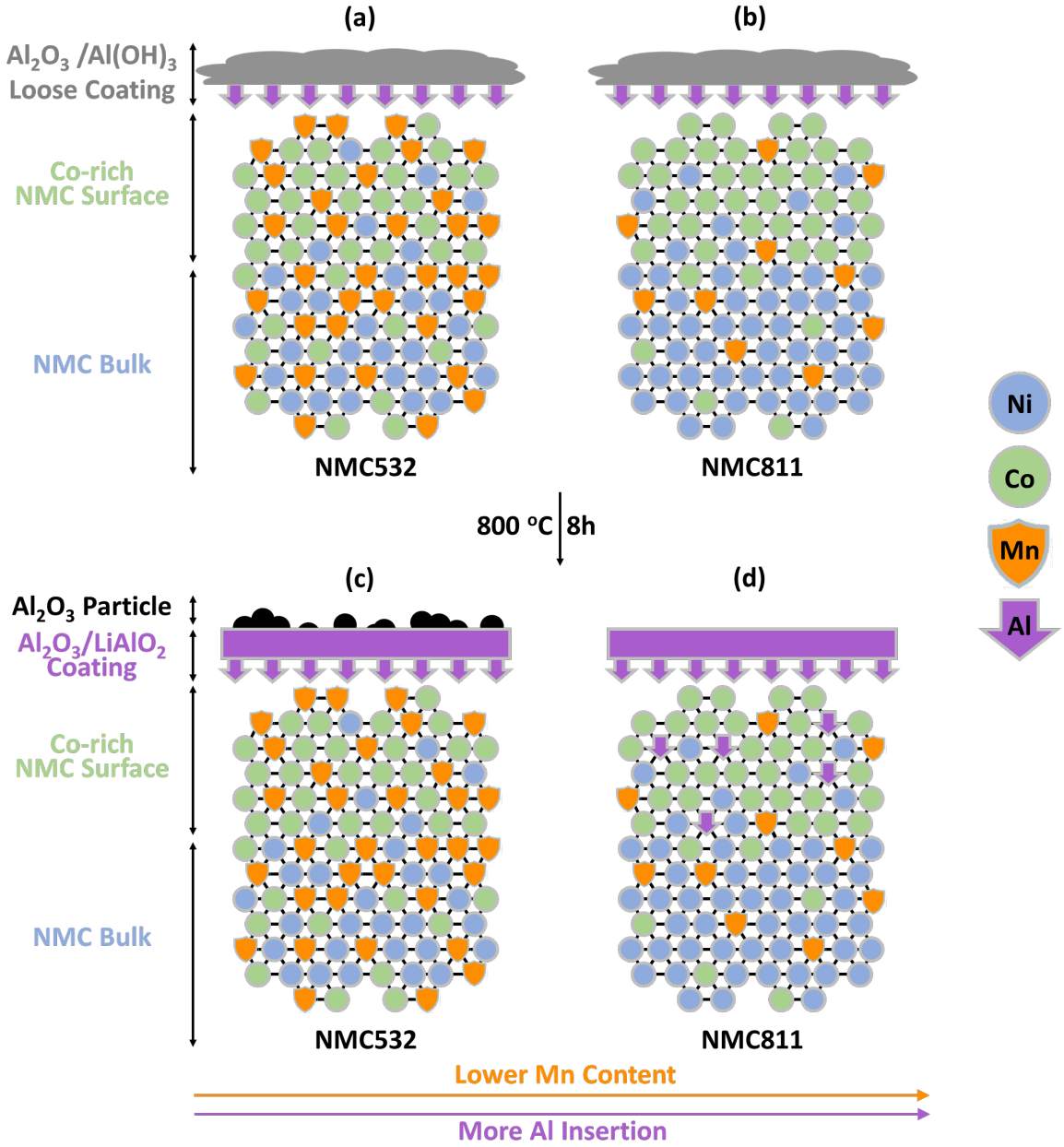

Figure 7. Scheme of the evolution of surface coating in Al_2O_3-coated (a)(c) NMC532 and (b)(d) NMC811. (a) and (b) are the scheme of as-coat particles, while (c) and (d) are the scheme of 800°C-annealed particles.

III.C. Electrochemical Test Results. Electrochemical characterization studies on coated NMC particles have shown that, the differences in interfacial composition, surface morphology and partial aluminum diffusion of different leads to differences in their electrochemical performance. The half-cell results of the pristine and coated NMC particles are shown in Figure S10 and Table S2, with a detailed analysis in the caption of Figure S10. In general, a good surface protection is achieved with Al_2O_3 coating on NMC532, but this protection effect is hindered when transition metal composition is changed to NMC622 or 811. One obvious difference is the diffusion of surface Al_2O_3 into the bulk, transforming the coating layer into a dopant, which no longer forms a protective layer outside the oxides to prevent the transition metal dissolution and/or oxygen leaching. In our previous study, we have shown that the aluminum diffusion from surface coating to the lattice for $LiCoO_2$ results poor cyclability[29]. Here a similar effect is observed for Ni-rich NCM cathodes whose surface is cobalt segregated. In addition, the diffusion of aluminum into the layered oxides may also disturb the surface crystal structure, create more dislocations and/or metal-Li exchange, and therefore result in lower capacity and cyclability.

IV. CONCLUSIONS

In this work, we systematically studied how the transition metal compositions in NMC cathode materials can influence the initial chemical and atomic structures of the surface, and consequently influence the reaction between the surface Al_2O_3 coating and bulk NMC oxides. Utilizing NMR, HRXRD, DFT calculations, and electron microscopy techniques, we have demonstrated that decreasing the Mn content in NMC materials facilities the diffusion of surface Al into the bulk, leading to a smoother surface after high-temperature annealing. Characterization studies also show that the initial surface lithium content, aluminum coating level and surface transition metal segregation affect the composition of the interfacial layer of coated particles. Al_2O_3-coated NMC532 does not show any aluminum insertion into the lattice and its initial surface Li is low. As a result, the high-temperature annealing leads to a protective $LiAlO_2$ shell only on the surface with excess Al_2O_3 aggregating into small particles decorated on the shell. For Al_2O_3-coated NMC622 and particularly NMC811 with lower Mn content in their transition metal layer, the coating turns to a dopant after high-temperature annealing, leading to a mixture of Al, Ni, and Co in transition metal layers close to surface layers with smaller or no scattered Al_2O_3 coating particles on the surface. The blocking effect of Mn on the Al insertion is confirmed by both experimental and computational results. Comparison studies with Al-doped layered oxides have shown that aluminum local ordering is independent of aluminum content and transition metal composition but depends on reaction kinetics. The electrochemical tests show that the diffusion of Al_2O_3 coatings into the bulk could

jeopardize the protection effect of Al_2O_3 coating and even cause a lower cyclability after coating. These discoveries demonstrate that the bulk composition could have a big influence on the structures and functions of the surface coating layers as well as bulk local ordering. Therefore, the compatibility between coating and core materials should be emphasized and carefully characterized in the future development of coated cathode materials.

ASSOCIATED CONTENT

Supporting Information

The Supporting Information is available free of charge on the Publications website at:
Electrochemical results, HRXRD results and refinement, DFT information, additional NMR, TEM, SEM and EELS results.

Author Information

Corresponding Author

*Email: binghong.han@anl.gov

Notes

The authors declare no competing financial interest.

ACKNOWLEDGEMENT

Support from the Vehicle Technologies Program, Hybrid and Electric Systems, in particular, David Howell, Tien Duong, and Peter Faguy, at the U.S. Department of Energy, Office of Energy Efficiency and Renewable Energy are gratefully acknowledged. The submitted manuscript has been created by UChicago Argonne, LLC, Operator of Argonne National Laboratory ("Argonne"). Argonne, a U.S. Department of Energy Office of Science laboratory, is operated under Contract No. DE-AC02-06CH11357. This work used SEM from the Electron Microscopy Center, TEM from the Center for Nanoscale Materials, and HRXRD from the Advanced Photon Source, all at Argonne, which are supported by the U. S. Department of Energy, Office of Science, Office of Basic Energy Sciences, also under Contract No. DE-AC02-06CH11357. Computer time allocations at the Argonne's Laboratory Computing Resource Center, is gratefully acknowledged. Dr. Jason Croy is acknowledged for valuable discussions and Dr. Cameron Peebles is acknowledged for experimental support for SEM images.

REFERENCES

(1) Tarascon, J. M.; Armand, M. Issues and Challenges Facing Rechargeable Lithium Batteries. *Nature* **2001,** *414*, 359-367.

(2) Weinstock, I. B. Recent Advances in the Us Department of Energy's Energy Storage Technology Research and Development Programs for Hybrid Electric and Electric Vehicles. *J. Power Sources* **2002,** *110*, 471-474.

(3) Blomgren, G. E. The Development and Future of Lithium Ion Batteries. *J. Electrochem. Soc.* **2017,** *164*, A5019-A5025.

(4) Jung, S.-K.; Gwon, H.; Hong, J.; Park, K.-Y.; Seo, D.-H.; Kim, H.; Hyun, J.; Yang, W.; Kang, K. Understanding the Degradation Mechanisms of $LiNi_{0.5}Co_{0.2}Mn_{0.3}O_2$ Cathode Material in Lithium Ion Batteries. *Adv. Energy Mat.* **2014,** *4*, 1300787.

(5) Shaju, K. M.; Subba Rao, G. V.; Chowdari, B. V. R. Performance of Layered $Li(Ni_{1/3}Co_{1/3}Mn_{1/3})O_2$ as Cathode for Li-Ion Batteries. *Electrochim. Acta* **2002,** *48*, 145-151.

(6) Jouanneau, S.; Eberman, K. W.; Krause, L. J.; Dahn, J. R. Synthesis, Characterization, and Electrochemical Behavior of Improved $Li[Ni_xCo_{1-2x}Mn_x]O_2$ ($0.1<X<0.5$) *J. Electrochem. Soc.* **2003,** *150*, A1637-A1642.

(7) Lu, Z.; MacNeil, D. D.; Dahn, J. R. Layered $Li[Ni_xCo_{1-2x}Mn_x]O_2$ Cathode Materials for Lithium-Ion Batteries. *Electrochem. Solid-State Lett.* **2001,** *4*, A200-A203.

(8) Liu, Z.; Yu, A.; Lee, J. Y. Synthesis and Characterization of $LiNi_{1-X-Y}Co_xMn_yO_2$ as the Cathode Materials of Secondary Lithium Batteries. *J. Power Sources* **1999,** *81–82*, 416-419.

(9) Yabuuchi, N.; Ohzuku, T. Novel Lithium Insertion Material of $LiCo_{1/3}Ni_{1/3}Mn_{1/3}O_2$ for Advanced Lithium-Ion Batteries. *J. Power Sources* **2003,** *119–121*, 171-174.

(10) Ohzuku, T.; Makimura, Y. Layered Lithium Insertion Material of $LiCo_{1/3}Ni_{1/3}Mn_{1/3}O_2$ for Lithium-Ion Batteries. *Chem. Lett.* **2001,** *30*, 642-643.

(11) Tran, N.; Croguennec, L.; Jordy, C.; Biensan, P.; Delmas, C. Influence of the Synthesis Route on the Electrochemical Properties of $LiNi_{0.425}Mn_{0.425}Co_{0.15}O_2$. *Solid State Ionics* **2005,** *176*, 1539-1547.

(12) Ma, M.; Chernova, N. A.; Toby, B. H.; Zavalij, P. Y.; Whittingham, M. S. Structural and Electrochemical Behavior of $LiMn_{0.4}Ni_{0.4}Co_{0.2}O_2$. *J. Power Sources* **2007,** *165*, 517-534.

(13) Shizuka, K.; Kobayashi, T.; Okahara, K.; Okamoto, K.; Kanzaki, S.; Kanno, R. Characterization of $Li_{1+Y}Ni_xCo_{1-2x}Mn_xO_2$ Positive Active Materials for Lithium Ion Batteries. *J. Power Sources* **2005,** *146*, 589-593.

(14) Wu, L.; Nam, K.-W.; Wang, X.; Zhou, Y.; Zheng, J.-C.; Yang, X.-Q.; Zhu, Y. Structural Origin of Overcharge-Induced Thermal Instability of Ni-Containing Layered-Cathodes for High-Energy-Density Lithium Batteries. *Chem. Mater.* **2011,** *23*, 3953-3960.

(15) Liang, C.; Kong, F.; Longo, R. C.; Kc, S.; Kim, J.-S.; Jeon, S.; Choi, S.; Cho, K. Unraveling the Origin of Instability in Ni-Rich $LiNi_{1-2x}Co_xMn_xO_2$ (NCM) Cathode Materials. *J. Phys. Chem. C* **2016,** *120*, 6383-6393.

(16) Konishi, H.; Yuasa, T.; Yoshikawa, M. Thermal Stability of $Li_{1-Y}Ni_xMn_{(1-X)/2}Co_{(1-X)/2}O_2$ Layer-Structured Cathode Materials Used in Li-Ion Batteries. *J. Power Sources* **2011,** *196*, 6884-6888.

(17) Sun, Y.-K.; Myung, S.-T.; Park, B.-C.; Prakash, J.; Belharouak, I.; Amine, K. High-Energy Cathode Material for Long-Life and Safe Lithium Batteries. *Nat. Mater.* **2009,** *8*, 320-324.

(18) Schipper, F.; Erickson, E. M.; Erk, C.; Shin, J.-Y.; Chesneau, F. F.; Aurbach, D. Review—Recent Advances and Remaining Challenges for Lithium Ion Battery Cathodes: I. Nickel-Rich, $LiNi_xCo_yMn_zO_2$. *J. Electrochem. Soc.* **2017,** *164*, A6220-A6228.

(19) Cho, W.; Kim, S.-M.; Song, J. H.; Yim, T.; Woo, S.-G.; Lee, K.-W.; Kim, J.-S.; Kim, Y.-J. Improved Electrochemical and Thermal Properties of Nickel Rich $LiNi_{0.6}Co_{0.2}Mn_{0.2}O_2$ Cathode Materials by SiO_2 Coating. *J. Power Sources* **2015,** *282*, 45-50.

(20) Chen, Y.; Zhang, Y.; Chen, B.; Wang, Z.; Lu, C. An Approach to Application for $LiNi_{0.6}Co_{0.2}Mn_{0.2}O_2$ Cathode Material at High Cutoff Voltage by TiO_2 Coating. *J. Power Sources* **2014,** *256*, 20-27.
(21) Wang, D.; Li, X.; Wang, Z.; Guo, H.; Huang, Z.; Kong, L.; Ru, J. Improved High Voltage Electrochemical Performance of Li_2ZrO_3-Coated $LiNi_{0.5}Co_{0.2}Mn_{0.3}O_2$ Cathode Material. *J. Alloy. Compd.* **2015,** *647*, 612-619.
(22) Cao, K.; Wang, L.; Li, L.; Liang, G. Effects of Al_2O_3 Coating on the Structural and Electrochemical Performance of $LiNi_{0.5}Co_{0.2}Mn_{0.3}O_2$ Cathode Material. *Appl. Mech. Mater.* **2013,** *320*, 235-240.
(23) Liao, J.-Y.; Manthiram, A. Surface-Modified Concentration-Gradient Ni-Rich Layered Oxide Cathodes for High-Energy Lithium-Ion Batteries. *J. Power Sources* **2015,** *282*, 429-436.
(24) Myung, S.-T.; Izumi, K.; Komaba, S.; Sun, Y.-K.; Yashiro, H.; Kumagai, N. Role of Alumina Coating on Li−Ni−Co−Mn−O Particles as Positive Electrode Material for Lithium-Ion Batteries. *Chem. Mater.* **2005,** *17*, 3695-3704.
(25) Shi, Y.; Zhang, M.; Qian, D.; Meng, Y. S. Ultrathin Al_2O_3 Coatings for Improved Cycling Performance and Thermal Stability of $LiNi_{0.5}Co_{0.2}Mn_{0.3}O_2$ Cathode Material. *Electrochim. Acta* **2016,** *203*, 154-161.
(26) George, S. M. Atomic Layer Deposition: An Overview. *Chem. Rev.* **2010,** *110*, 111-131.
(27) Riley, L. A.; Van Atta, S.; Cavanagh, A. S.; Yan, Y.; George, S. M.; Liu, P.; Dillon, A. C.; Lee, S.-H. Electrochemical Effects of Ald Surface Modification on Combustion Synthesized $LiNi_{1/3}Mn_{1/3}Co_{1/3}O_2$ as a Layered-Cathode Material. *J. Power Sources* **2011,** *196*, 3317-3324.
(28) Dogan, F.; Vaughey, J. T.; Iddir, H.; Key, B. Direct Observation of Lattice Aluminum Environments in Li Ion Cathodes $LiNi_{1-y-z}Co_yAl_zO_2$ and Al-Doped $LiNi_xMn_yCo_zO_2$ Via ^{27}Al MAS NMR Spectroscopy. *ACS Appl. Mater. Interfaces* **2016,** *8*, 16708-16717.
(29) Han, B.; Peebles, C.; Paulauskas, T.; Park, J.-S.; Key, B.; Vaughey, J. T.; Dogan, F. Understanding the Role of Temperature and Cathode Composition on Interface and Bulk: Optimizing Aluminum Oxide Coatings for Li-Ion Cathodes. *ACS Appl. Mater. Interfaces* **2017,** *9*, 14769–14778.
(30) *Topas V5. General Profile and Structure Analysis Software for Powder Diffraction Data. User's Manual*. Karlsruhe: Bruker AXS: **2015**.
(31) Kresse, G.; Furthmüller, J. Efficiency of Ab-Initio Total Energy Calculations for Metals and Semiconductors Using a Plane-Wave Basis Set. *Computational Materials Science* **1996,** *6*, 15-50.
(32) Kresse, G.; Hafner, J. Ab Initio. *Phys. Rev. B* **1993,** *47*, 558-561.
(33) Perdew, J. P.; Burke, K.; Ernzerhof, M. Generalized Gradient Approximation Made Simple. *Physical Review Letters* **1996,** *77*, 3865-3868.
(34) Blöchl, P. E. Projector Augmented-Wave Method. *Phys. Rev. B* **1994,** *50*, 17953-17979.
(35) Iddir, H.; Benedek, R. First-Principles Analysis of Phase Stability in Layered–Layered Composite Cathodes for Lithium-Ion Batteries. *Chem. Mater.* **2014,** *26*, 2407-2413.
(36) Heyd, J.; Scuseria, G. E.; Ernzerhof, M. Hybrid Functionals Based on a Screened Coulomb Potential. *The Journal of Chemical Physics* **2003,** *118*, 8207-8215.
(37) Yan, P.; Zheng, J.; Zheng, J.; Wang, Z.; Teng, G.; Kuppan, S.; Xiao, J.; Chen, G.; Pan, F.; Zhang, J.-G.; Wang, C.-M. Ni and Co Segregations on Selective Surface Facets and Rational Design of Layered Lithium Transition-Metal Oxide Cathodes. *Adv. Energy Mat.* **2016,** *6*, 1502455.
(38) Grey, C. P.; Dupré, N. Nmr Studies of Cathode Materials for Lithium-Ion Rechargeable Batteries. *Chem. Rev.* **2004,** *104*, 4493-4512.
(39) Cahill, L. S.; Yin, S. C.; Samoson, A.; Heinmaa, I.; Nazar, L. F.; Goward, G. R. 6li Nmr Studies of Cation Disorder and Transition Metal Ordering in $Li[Ni_{1/3}Mn_{1/3}Co_{1/3}]O_2$ Using Ultrafast Magic Angle Spinning. *Chem. Mater.* **2005,** *17*, 6560-6566.
(40) Solomon, I. Relaxation Processes in a System of Two Spins. *Physical Review* **1955,** *99*, 559-565.
(41) Liu, H.; Bugnet, M.; Tessaro, M. Z.; Harris, K. J.; Dunham, M. J. R.; Jiang, M.; Goward, G. R.; Botton, G. A. Spatially Resolved Surface Valence Gradient and Structural Transformation of Lithium Transition Metal Oxides in Lithium-Ion Batteries. *Phys. Chem. Chem. Phys.* **2016,** *18*, 29064-29075.

TOC GRAPHIC

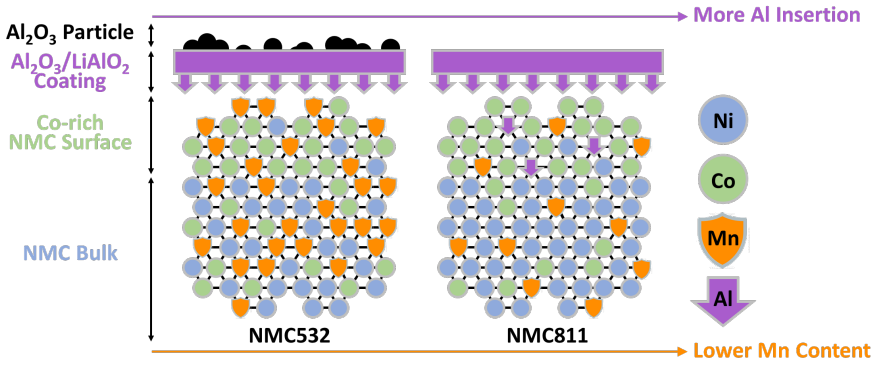
More Al Insertion
Al_2O_3 Particle
$Al_2O_3/LiAlO_2$ Coating
Co-rich NMC Surface
NMC Bulk
Ni
Co
Mn
Al
NMC532
NMC811
Lower Mn Content